Lunasin Soy Peptide Inhibition of Melanoma *in-vitro*

Matthew Bienick, Christopher Shidal, B.S. and Keith Davis, Ph. D.
UofL Departments of Pharmacology and Toxicology

James Graham Brown Cancer Center
A proud member of UofL Health Care

Abstract

We are currently investigating the effects of lunasin's ability to inhibit the proliferation of melanoma cells *in vitro*. Lunasin, a soy peptide consisting of 44 amino acids, decreases proliferation of several cancer types. Since its isolation in 1999, numerous studies have revealed its mechanism of action is through interactions with core histone tails (i.e. H3 and H4), where it binds to lysine residues to competitively inhibit binding of histone acetyltransferases (HATs) involved in activation of transcription. Three common domains in the peptide chain are attributed for lunasin's ability to localize and diminish HAT activity; a helical region, an RGD motif, and a poly-aspartic acid tail.

PLX4032 (Vemurafenib) is a B-RAF inhibitor that alters signaling of the MAPK pathway. A mutant form of B-RAF known as B-RAF V600E, is constitutively active due to the replacement of valine with glutamic acid at the 600th amino acid residue. PLX4032 is able to selectively arrest the proliferation of cells that contain this mutant form of B-RAF. Unfortunately, clinical research has shown that after initial tumor regression in patients responding to treatment, tumors metastasize and progress with little sensitivity to ongoing vemurafenib treatments.

It is hypothesized that combination treatment of lunasin with PLX4032 will produce a synergistic antiproliferative effect using established melanoma cell lines as a model. Specific melanoma cell lines were chosen to have the V600E mutation. Not only do we expect lunasin and PLX4032 to interact cooperatively to abolish the ability of melanoma cell lines to form tumors, but to sensitize resistant strains to vemurafenib treatment as well.

Initial results suggest that lunasin and PLX4032 interact synergistically in soft agar colony forming assays and additively in spheroid assays, depending on cell line. Combination treatment in 2-D proliferation assays had a slightly antagonistic effect on SKMEL-28 cells, an additive effect on A375 cells, and a synergistic effect on A375R cells. Assessment of calculated DI values reveals a broad spectrum of interactions between lunasin and vemurafenib, which is reliant upon dose ratio and cell line. Future experiments are needed to determine the exact mechanisms of this interaction and extrapolate clinically relevant data for sensitizing PLX4032 resistant cells with lunasin co-treatment.

Results

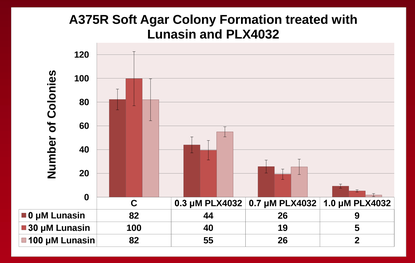

Figure 2. A375R colony counts for treatments of lunasin, PLX4032, and combination. A375R cells were synergistically effected by combination treatment with various PLX4032 concentrations at 30µM lunasin. Combination treatments of 100µM lunasin show a slight additive effect with 0.7µM and 0.3µM PLX4032 and a strong synergestic effect at 1.0µM.

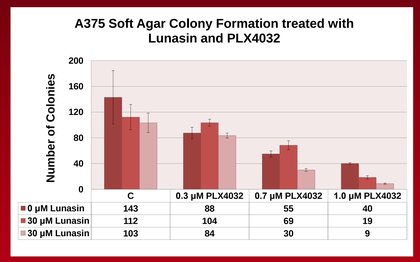

Figure 3. A375 colony counts for treatments of lunasin, PLX4032, and combination. Combination treatment of both 30µM and 100µM lunasin showed an increasingly synergistic effect on the A375 cells as the concentration of PLX4032 increased.

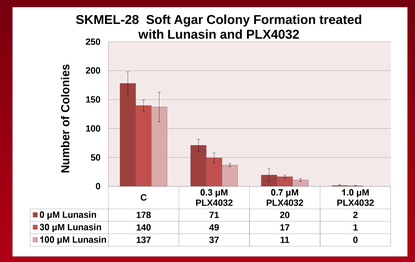

Figure 4.SKMEL-28 colony counts for treatments of lunasin, PLX4032, and combination. Drewinko index calculations showed that combination treatment of lunasin and PLX4032 have a strong synergistic affect on SKMEL-28 cells.

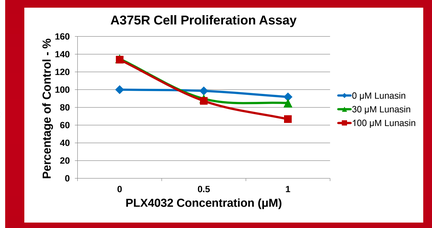

Figure 5. A375R proliferation assay for treatments of lunasin, PLX4032, and combination. Both 30µM and 100µM lunasin in combination with PLX4032 showed Drewinko Index values that indicate a strong synergistic effect on A375R cells.

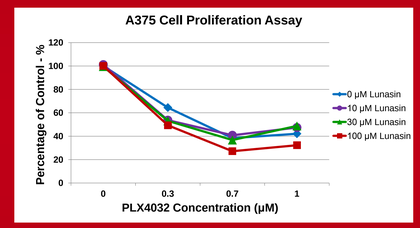

Figure 6. A375 proliferation assay for treatments of lunasin, PLX4032, and combination. 30µM and 10µM lunasin with PLX4032 showed an additive effect, while 100µM lunasin in combination with PLX4032 revealed a synergistic effect on A375 cells.

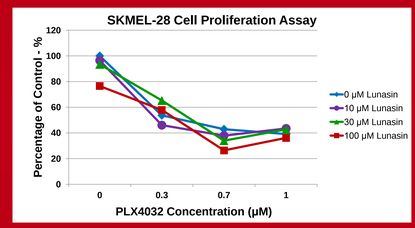

Figure 7. A375 proliferation assay for treatments of lunasin, PLX4032, and combination. All combination treatments of lunasin and PLX4032 showed an antagonistic effect to inhibiting SKMEL-28 proliferation, except for lunasin in combination with 0.7 µM PLX4032. The various concentrations of lunasin and 0.7 µM PLX4032 all had a synergistic effect of inhibiting cell proliferation.

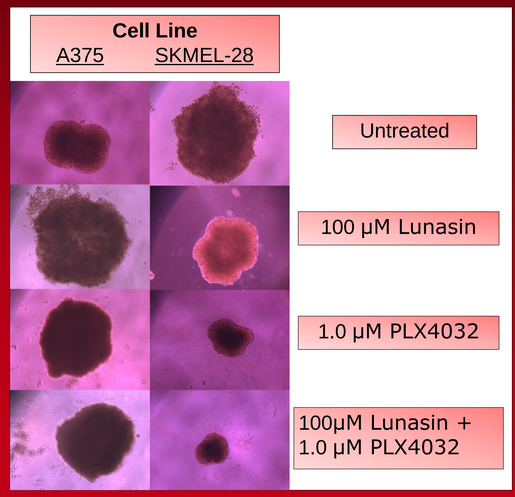

Figure 10. Spheroid formation was affected by lunasin and PLX4032 treatments. Lunasin partially reduced spheroid formation in the SKMEL-28 strain and in combination with PLX4032. In the A375, Lunasin partially inhibits formation of spheroids. The packing of cells were less dense than compared to the SKMEL-28. Therefore, the spheroid sizes were larger with treatments of lunasin. Pictures taken at +96 hours after treatment.

Mechanism of Action

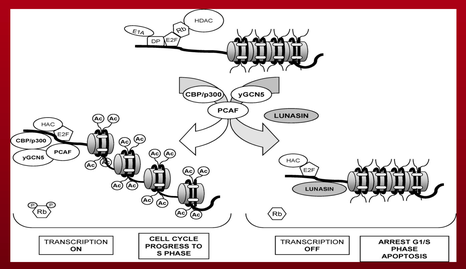

1. Helical Region: Chromatin Binding*
2. RGD Motif: Internalization
3. Poly D tail: Histone binding (H3 and H4)

SKWQHQQDSCRKQLQGVNLTPCEKHIMEKIQGRGDDDDDDDDN

Figure 1. Lunasin interacts with H3 and H4 histone tails to competitively inhibit binding of HATs. It has three domains which contribute to its ability to internalize and bind the tails.

Methods

Soft Agar Assays: measured the ability of treated cells to form colonies in a 3-D matrix. Cells were treated with lunasin, PLX4032, and co-treatment. Colony counts were performed 2-4 weeks after treatment depending on cell line.

CellTiter 96® AQ_{ueous} Non-Radioactive Cell Proliferation (MTS) Assay: measured proliferative ability of cells in 2D 96-well format after treatments that alter epigenetic modifications. Assays were ran for 72 hours.

Spheroid Assays cells form spheroids in a 3-D matrix. This assay measures the cells ability to congregate and form spheroids after exposure to epigenetic altering drugs. Jimage software from NIH was used for area measurements.

Calculation of Drewinko Index (DI): analysis of interactions between compounds. DI <1 is less than additive (antagonistic), = 1 is additive, and >1 is more than additive (synergistic).

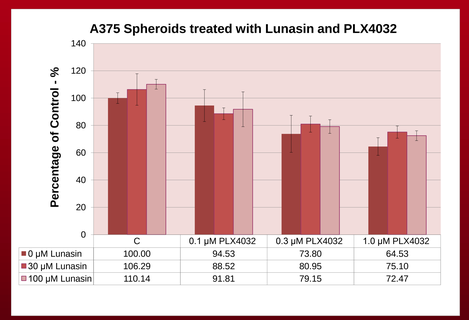

Figure 8. A375 spheroid size as a percentage of the control with treatment of lunasin, PLX4032, and combination. Using the Drewinko index, it was found that lunasin combination treatment with PLX4032 was only slightly additive. Lunasin treatment alone did not inhibit spheroid growth..

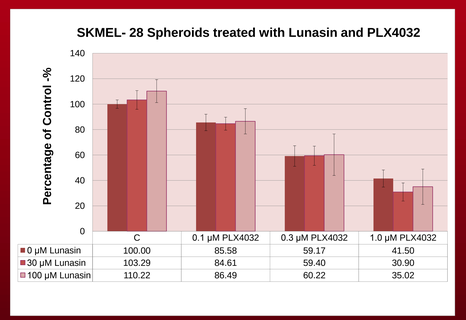

Figure 9. SKMEL-28 spheroid size as a percentage of the control with treatment of lunasin, PLX4032, and combination. The Drewinko index values showed that lunasin combination treatment with PLX4032 was only slightly additive. Lunasin treatment alone did not significantly alter spheroid area.

Conclusions

- Lunasin inhibits cancer cell proliferation *in-vitro* and interacts synergistically in soft agar assays in combination with PLX4032
- Combination treatment of lunasin with PLX4032 in cell proliferation assays had various effects on inhibiting cell proliferation and were dependent upon cell line and dose ratios
- Lunasin interacts only slightly additively in spheroid assays in combination with PLX4032
- Further research is warranted into the mechanisms of this interaction between therapeutic treatments

Future Plans

- Migration and invasion transwell assays
- *In-vivo* models measuring suppression of tumor growth by lunasin and histopathology

Acknowledgements

Research supported by
- University of Louisville Cancer Education Program
- Grant R25-CA1344238 from the National Cancer Institute/ NIH

Acetylator Genotype-Dependent N-acetylation of Isoniazid in Human Hepatocytes In Situ

Srineil Bodduluri, B.S., Mark A. Doll, M.S., Raúl Alejandro Salazar González, M.S. and David W. Hein, Ph.D.

Department of Pharmacology and Toxicology and James Graham Brown Cancer Center, University of Louisville

Abstract

Hepatotoxicity is a common symptom among patients undergoing treatment for tuberculosis that may progress to liver cancer. Clinical studies have recommended that a genotype dependent "pharmacogenetic" approach be used in determining a dose required for successful treatment and minimization of toxicity. N-acetyltransferase 2 (NAT2) is the primary enzyme involved in the metabolism of the anti-tuberculosis drug isoniazid and is subject to genetic polymorphism in human populations resulting in rapid, intermediate, and slow acetylator phenotypes. NAT2-genotype-dependent metabolism of isoniazid to date has not been observed in liver hepatocytes in situ. *NAT2* genotype in the cryopreserved hepatocytes was determined by Taqman allelic discrimination assay of genomic DNA. Cryoplateable human hepatocytes from three rapid NAT2 acetylator genotype (*NAT2*4/*4*, **12A/*12A* and **4/*4*), intermediate acetylator genotype (*NAT2*4/*6A*, **4/*5B* and **4/*7B*), and slow acetylator genotype (*NAT2*5B/*5B*, **5B/*6A* and **6A/*6A*) were thawed, plated and equilibrated 24 hr. prior to isoniazid exposure. The production of acetyl-isoniazid in the media was measured by high performance liquid chromatography up to 48 hr. Human hepatocytes cultured in situ demonstrated a dose-dependent (10-200 µM) and time-dependent (0 - 48 hrs) increase in acetyl-isoniazid. When comparing the amount of acetyl-isoniazid produced/24hr/ millions cells among the various samples, a robust and significant ($p<0.001$) NAT2 acetylator genotype dependent difference was observed in production of N-acetyl-isoniazid, with rapid NAT2 acetylator hepatocytes producing the highest amounts of acetyl-isoniazid followed by intermediate acetylators and slow acetylators following exposures to both 12.5 and 100 µM isoniazid.

Introduction

Therapeutic drug induced hepatotoxicity is a common symptom among patients undergoing treatment for tuberculosis. Numerous clinical studies have recommended that a genotype dependent "pharmacogenetic" approach be used in determining a dose required for successful treatment. Specifically, patients with an arylamine N-acetyltransferase 2 (NAT2) slow acetylator profile are recommended to take a lower dose to prevent hepatotoxicity while patients with a NAT2 rapid acetylator profile are permitted to take a higher dose to fight infection. NAT2 is the main enzyme involved in the metabolism of the anti-tuberculosis drug isoniazid.

Study Objective

- To determine whether primary human hepatocytes cultured in situ are able to metabolize isoniazid to acetyl-Isoniazid in a time, dose and N-acetyltransferase 2- genotype dependent manner.

Materials and Methods

Human hepatocytes were obtained from BioreclamationIVT, Baltimore, MD. Upon receipt, hepatocytes were stored in liquid nitrogen until use. Upon removal from the liquid nitrogen, the hepatocytes were thawed and centrifuged as described by supplier. Genomic DNA was isolated from pelleted cells using the QIAamp® DNA Mini Kit (Qiagen, MD, USA) according to manufacturer's instructions. SNPs in the *NAT2* coding region and their corresponding alleles and haplotypes were determined with the seven-SNP panel assay as previously described. Briefly, SNP-specific PCR primers and fluorogenic probes were designed using Primer Express™ (Applied Biosystems, CA, USA). The fluorogenic probes are labeled with a reporter dye (either carboxyfluorescein or VIC®, Applied Biosystems) and are specific for one of the two possible bases identified at the seven SNPs rs1801279 (191G>A), rs1041983 (282C>T), rs1801280 (341T>C), rs1799929 (481C>T), rs1799930 (590G>A), rs1208 (803A>G) and rs1799931 (857G>A) in the *NAT2* coding region. Upon removal from the liquid nitrogen, the hepatocytes were thawed and plated on collagen-coated 12 well plates according to supplier's protocols. Hepatocytes were plated and cells allowed to attach for 24hr prior to the addition of Isoniazid. Isoniazid was dissolved and diluted in hepatocytes plating media for all experiments. Plated hepatocytes were incubated with media containing isoniazid at concentration from 10 to 200 µM for up to 48 hrs. An aliquot of the hepatocytes media was removed at different time point to measure the production of acetyl-isoniazid. The amount of acetyl-isoniazid produced was determined following separation and quantitation by high performance liquid chromatography. Separation of isoniazid and Acetyl-isoniazid were done using a 125 X4 mm lichrosher 100 RP-100 5µM C18 HPLC column. We used an isocratic gradient of 86% 25 mM sodium phosphate, 10 mM heptane sulfonate pH 3.0 for 6 min. Retention times for Isoniazid and acetyl-isoniazid were 2.63 min and 2.93 min respectively.

SNP's that Result in Alleles with Reduced Activity

191G>A **341T>C** **590G>A** **857G>A**

Slow Acetylator Alleles Resulting from the Presence of the Above SNPs Respectively

NAT2*14 ***NAT2*5*** ***NAT2*6*** ***NAT2*7***

Individuals Possessing **NONE** of the Above 4 Alleles are **RAPID** Acetylators

Individuals Possessing **ONE** of the Above 4 Alleles are **INTERMEDIATE** Acetylators

Individuals Possessing **TWO** of the Above 4 Alleles are **SLOW** Acetylators

Figure 1. Relationship between SNPs in N-acetyltransferase-2 gene, their corresponding alleles and resulting phenotype.

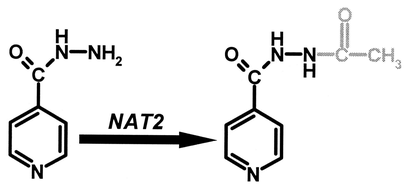

Isoniazid **Acetyl-Isoniazid**

Figure 2. Conversion of Isoniazid to Acetyl-Isoniazid by Arylamine N-acetyltransferase 2 in the presence of acetyl-coenzyme A

Results

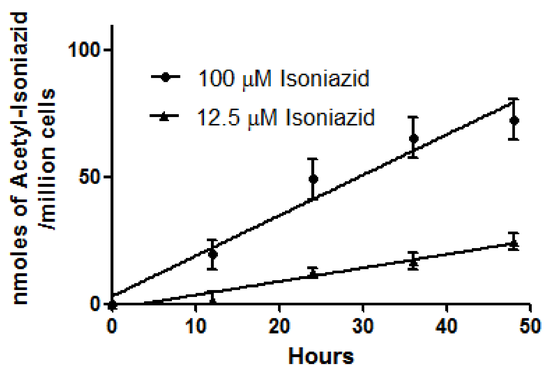

FIGURE 3. Time course for the in situ N-acetylation of isoniazid in primary human hepatocytes. The following graph illustrates the increase in acetyl-isoniazid levels over time. It shows a linear increase in the amount of acetyl-isoniazid over the course of a 50 hour period.

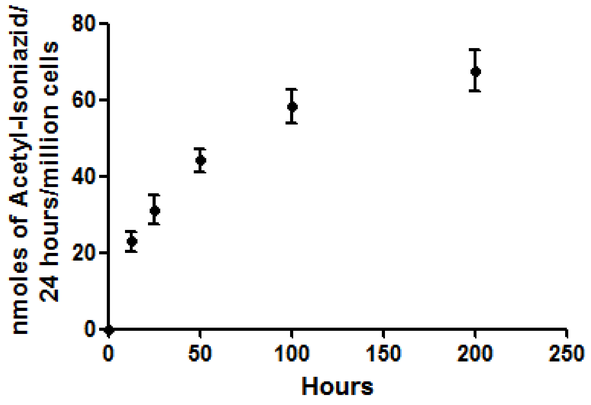

FIGURE 4. In situ concentration dependent N-acetylation of isoniazid in primary human hepatocytes. The following graph illustrates the relationship between the concentration of isoniazid administered and the amount of acetyl-isoniazid produced after 24 hours. Five different concentrations of isoniazid were used. The levels of acetyl-isoniazid seem to plateau at about 100uM of isoniazid. This could possibly be due to NAT 2 enzyme saturation with substrate.

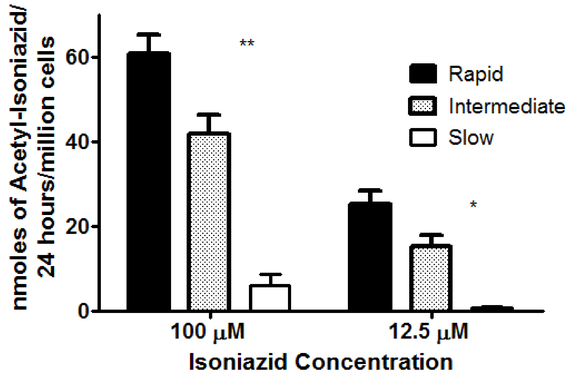

FIGURE 4 In situ metabolism of isoniazid in primary human hepatocytes from rapid, intermediate and slow acetylators. The following graph illustrates the differences in isoniazid metabolism based on acetylator status. The levels of acetyl-isoniazid after a 24 hour period was measured for rapid, intermediate, and slow acetylators. As predicted, rapid acetylators produced the highest levels of acetyl-isoniazid followed by intermediate and slow acetylators. Differences between rapid, intermediate, and slow acetylators differed significantly at both 100 (** $p=0.0002$) and 12 (*$p=0.0023$) µM.

Conclusions

- The concentration of acetyl-isoniazid increases linearly over a 48 hour period after a single dose exposure to isoniazid.
- The concentration of acetyl-isoniazid increases proportionately as the concentration of isoniazid increases up until a threshold point where it plateaus, presumably due to the saturation of the enzyme NAT2.
- Hepatocytes expressing the rapid acetylator phenotype produced the largest amount of acetyl-isoniazid over a 24 hour period, followed by intermediate acetylators, and then slow acetylators.
- Further in situ toxicity studies of anti-tuberculosis drugs on primary hepatocytes are needed to uncover more information about drug induced hepatotoxicity.
- Partially supported by National Cancer Institute grant R25-CA-134283.

UNIVERSITY OF LOUISVILLE
It's Happening Here.®

Gene Expression Alterations in Breast Carcinomas from Patients with Racial Differences

Adrienne M. Bushau, Sarah A. Andres and James L. Wittliff

Department of Biochemistry & Molecular Biology, Brown Cancer Center and Institute for Molecular Diversity & Drug Design, University of Louisville, Louisville, KY 40292

Abstract:

Background: African American women often exhibit more aggressive breast cancers and have a higher mortality rate than Caucasian women. Socioeconomic variances in racial groups do not explain many of the differences observed in clinical behavior of breast carcinomas. Our goal is to determine dissimilarities in gene expression of breast carcinoma biopsies of white and black patients and to evaluate their relationship to cancer behavior.

Materials and Methods: Using an IRB-approved biorepository and database, gene expression levels were compared in biopsies from white and black patients utilizing microarray analyses of LCM-procured carcinoma cells. Frozen tissue sections of primary breast carcinomas from de-identified patients were utilized for qPCR analyses. Total RNA was extracted with the RNeasy® Mini Kit (Qiagen), evaluated with the Bioanalyzer (Agilent) and reverse transcribed using iScript (Biorad). QPCR was performed using Power Sybr® Green (Applied Biosystems) and relative expression was calculated using Universal Human Reference RNA (Stratagene) as the calibrator and ACTB for normalization.

Results: Examination of microarray results of candidate genes revealed that expression levels of CARD11, TRAPPC2L, CRYBB2P1 and PDHA1 were significantly different in carcinomas of African American patients compared to those of Caucasian patients. Of these genes, PDHA1 expression was correlated with overall survival (P=0.05) when the entire population of 245 breast carcinoma patients was stratified by median expression level without regard to race. Furthermore, PDHA1 expression assessed by microarray was correlated with overall survival of white patients (P=0.04) when stratified by race and gene expression level. Using qPCR of RNA from intact tissue sections, expression levels of PDHA1, CRYBB2 and TRAPPC2L were analyzed for correlation with survival outcomes. When the entire patient population was stratified by median gene expression level, PDHA1, CRYBB2 and TRAPPC2L were not statistically significant for associations with disease-free or overall survival. However, when stratified by race and median gene expression, increased expression of TRAPPC2L was correlated with longer disease-free survival (P=0.002, HR=8.84) in black patients.

Conclusions: Expression levels of CARD11, PDHA1, TRAPPC2L and CRYBB2P1 were significantly different in breast tissue biopsies of African American patients when compared to those of Caucasian patients. Of the four genes, only PDHA1 gene expression levels of LCM-procured carcinoma cells were significant when correlated with overall survival of the entire population (n=245) regardless of race. Furthermore, PDHA1 expression was correlated with overall survival when only white patients were considered. Although dissimilarities in gene expression levels were observed in black and white patients, preliminary evaluation of a limited gene subset to personalize prognosis assessment requires additional studies related to a patient's ethnical background.

Introduction:

Numerous studies have shown that African American women often have a more aggressive breast cancer and have a higher mortality rate than Caucasian women. A difference in cultural and socioeconomic status is one explanation for African Americans presenting a higher mortality rate and a more advanced stage of breast cancer than Caucasian patients. However, some studies have shown that differences in insurance coverage and socioeconomic status do not explain the observed differences seen between blacks and whites (1). Through this information, it is valid to suspect biological differences affecting breast cancer in black and white patients. Breast tumors may be classified using five immunohistochemical (IHC) tumor markers: estrogen receptor (ER), progesterone receptor (PR), and human epidermal growth factor receptor-2 (HER2) (2). Estrogen and progesterone receptors play an important role in predicting prognosis and response to endocrine therapy in breast cancer. Hormone receptor-negative breast tumors are associated with poorer survival, whereas tumors that have a lobular history are associated with better survival (1). Almost two thirds of ER- positive patients respond favorable to endocrine therapy; less than ten percent of ER-negative patients exhibit a favorable response to endocrine therapy (1). Previous studies have shown that African Americans are more likely to have ER-negative, PR-negative breast tumors (2). This study primarily focused on the discrepancies in gene expression involved in white and black breast cancer patients.

Materials and Methods

Tissue Preparation & RNA Extraction

Using an IRB-approved study, frozen tissue sections from de-identified patients diagnosed with primary breast carcinoma and metastasis were utilized. Total RNA was extracted from frozen intact tissue sections with the RNeasy® Mini Kit (Qiagen Inc., Valencia, CA). Integrity of RNA was analyzed using the Bioanalyzer 2100 (Agilent Technologies, Palo Alto, CA). Total RNA was reverse transcribed using iScript (Biorad, Hercules, CA).

Gene Expression Analyses

Primers were designed using Primer Express (Applied Biosystems) and Primer Blast (NCBI). RNA quantification and analyses were performed in triplicate by qPCR in duplicate wells using the ABI Prism® 7900HT (Applied Biosystems, Foster City, CA) with Power Sybr® Green (Applied Biosystems) for detection. Relative gene expression was calculated using the ΔΔCt method with cDNA prepared from Universal Human Reference RNA (Stratagene, La Jolla, CA) as both a calibrator and a standard for quantification of RNA using β-actin (ACTB) as a reference gene.

Statistical Analysis

T-test, Kaplan Meier Plots, and Tumor Marker Analyses were performed in Graph Pad Prism. Pearson Correlations were performed in SPSS Statistics 20. The gene interaction analyses were performed through Ingenuity IPA.

Figure 1: Kaplan-Meier Plots of Black vs White Patients without Regard to Gene Expression Levels

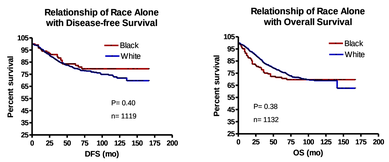

Figure 2: Box and Whisker Plots of Tumor Marker Levels of Patients with Differing Ethnical Heritage

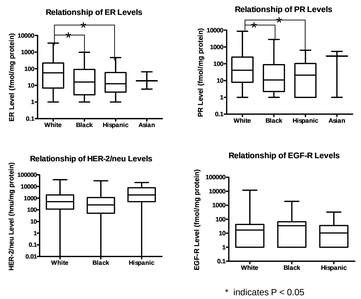

* indicates P < 0.05

Table 1: Results of T-Test of Microarray Data Comparing Gene Expression Levels in Patients with Differing Racial Backgrounds

(Most Significant Genes are Shown)

Gene ID	T-test (P-value)
PSPH	7.07 E-11
TRAPPC2L	5.36 E-10
PCSK4	4.61 E-08
DPH2	4.18 E-07
CARD11	4.87 E-07
SLIT3	5.90 E-07
PLEKHA8	9.12 E-07
PDHA1	9.37 E-07
CRYBB2P1	9.37 E-07
HAMP	9.78 E-07
SLC22A1	1.20 E-06
CST5	1.39 E-06
DCSTAMP	1.53 E-06
GLS2	2.67 E-06
WDR48	2.87 E-06
A4GNT	4.68 E-06
CGB1	4.88 E-06
KRTAP3-3	5.60 E-06
POLRIA	5.66 E-06
PNO1	8.02 E-06

Figure 3: Box and Whisker Plots of Expression Levels of Candidate Genes from Microarray

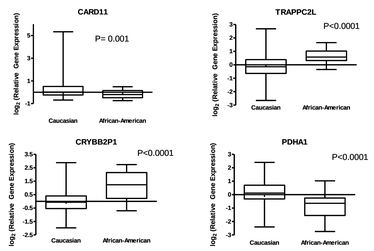

The box represents gene expression levels within the second and third quartiles of values observed. The horizontal line within the box represents the median expression level, while the whiskers extend to the lowest and highest expression level for each gene.

Figure 4: Kaplan-Meier Plots of Patients Stratified by Levels of Expression of the Candidate Genes without Regard to Race (n = 245)

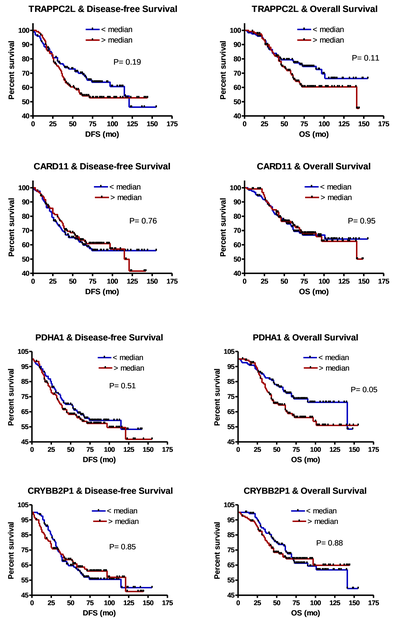

Figure 5: Kaplan-Meier Plots of Patients Stratified by Levels of Expression of the Candidate Genes & Patient Race (n = 245)

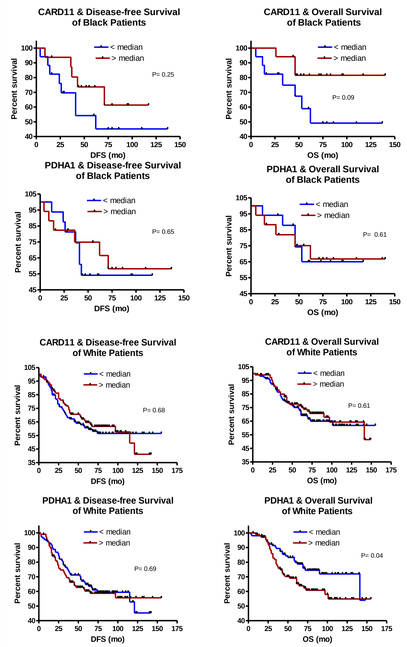

Figure 6: Comparison of Expression Levels of Candidate Genes Measured by Microarray and qPCR (n = 48)

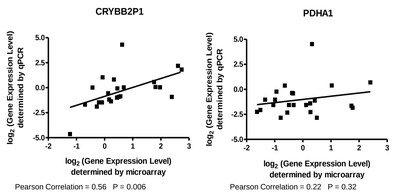

Figure 7: Kaplan-Meier Plots of Patient Survival in Relation to Gene Expression Levels Measured by qPCR

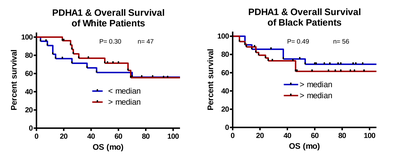

Figure 8: Gene Interactions Identified using Ingenuity Pathway Analysis (Genes of Interest indicated by Shaded Areas)

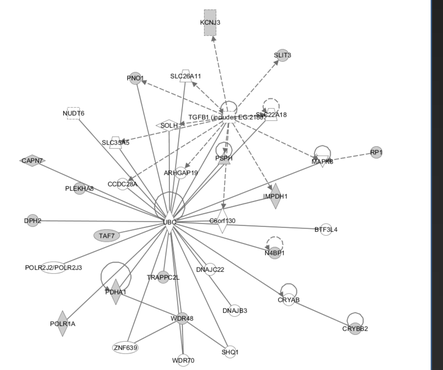

Conclusions:

- Patient survival did not appear to be correlated with race when the overall population was considered (n = 1132).
- ER and PR protein levels were significantly different in carcinomas of white, black and hispanic patients, but no differences were observed in HER-2/neu or EGF-Receptor protein levels.
- Comparisons of gene expression levels in breast carcinomas from patients with different ethnical backgrounds identified 475 genes with P < 0.01 and 116 genes with P < 0.001 using microarray data.
- Candidate genes from microarray data were analyzed further: CARD11, PDHA1, TRAPPC2L and CRYBB2P1 expression levels were significantly different in tissue biopsies when compared to patient ethnical heritage.
- PDHA1 gene expression in LCM-procured carcinoma cells was significantly correlated with overall survival of the study population regardless of race.
- PDHA1 expression in LCM-procured carcinoma cells was correlated with overall survival only in white patients.
- CARD11, TRAPPC2L and CRYBB2P1 expression did not appear to be correlated with patient survival in patients of different ethnical heritage.
- Gene expression was also evaluated by qPCR in a subset of patients for further analysis.
- Evaluation of a limited gene subset suggests additional studies are warranted to determine the relationship of a breast cancer patient's ethnical background to personalize prognosis assessment.

References:

1. Li CI et al. Differences in Breast Cancer Hormone Receptor Status and Histology by Race and Ethnicity among Women 50 Years of Age and Older. Cancer Epidemiol Biomarkers Prev 11:601-607, 2002.
2. O'Brien KM et al. Intrinsic Breast Tumor Subtypes, Race, and Long-term Survival in the Carolina Breast Cancer Study. Clin Cancer Res 16: 6100-6110, 2010.
3. Ma XJ et al. Gene expression associated with clinical outcome in breast cancer via laser capture microdissection. Breast Cancer Res Treat 82, 2003.
4. Mohla S et al. Estrogen and Progesterone Receptors in Breast Cancer in Black Americans: Correlation of Receptor Data with Tumor Differentiation. Cancer 50:552-9, 1982.
5. Wittliff JL et al. Gene expression profiles and tumor marker signatures of human breast carcinoma cells procured by laser capture microdissection. Endocrine Soc Abs P3-198, 2002.
6. Wittliff JL et al. Expression of estrogen receptor-associated genes in breast cancer cells procured by laser capture microdissection. Jensen Symp Abs 81, 2003.

Acknowledgements:

AMB was supported by a fellowship from the NCI R25 grant support University of Louisville Cancer Education Program NIH/NCI (R25-CA134283).

A microgenomic approach to identify clinically relevant gene signatures that discriminate between invasive lobular and ductal breast carcinomas

Sean T. Butterbaugh[1], Sarah A. Andres[1], Mary Ann Sanders[2], James L. Wittliff[1]

[1]Department of Biochemistry & Molecular Biology, [2]Department of Pathology, University of Louisville, Louisville, KY 40202

Abstract:

In an effort to distinguish between the two most common invasive breast carcinomas, lobular (ILC) and ductal (IDC), we searched for a genomic marker that discriminates these histologic types when conventional tests are conflicting. A specific genomic marker would be useful to distinguish IDC from ILC, due to the varied responses of luminal A-like-IDC and ILC to the aromatase inhibitor letrozole in post-menopausal women [Metzger et al. Cancer Res 2012]. Although CGH analysis shows that ILC is closely related to low grade IDC (luminal A-like) and genetically unrelated to intermediate and high grade IDC [Reis-Filho, 2005], ILC response to letrozole is more like luminal-B-like IDC (intermediate or high grade). To identify candidate genes, microarray analysis of expression levels were evaluated in laser capture microdissected carcinoma cells of biopsies that were positive for estrogen (ER) and progesterone receptors (PR). In low grade IDC and ILC, 299 probes were differentially expressed ($p<0.01$), and 99 of these probes were not differentially expressed ($p>0.01$) between high grade IDC and ILC. These 99 genes serve as candidates for a genomic marker differentiating these two histologic types. Microarray results showed varying expression levels of BRWD1, CAPSL, CHRNA7, CMTM7, CRMP1, GSKIP, HBEGF, PAPPA, and LRBA among the different cancer pathologies. By using quantitative polymerase chain reaction (qPCR), we determined expression levels relative to ACTB for the gene candidates in order to validate those from the microarray array results. qPCR analyses are used to validate and refine the gene subset distinguishing ILC from low grade IDC. Our novel approach is revealing microgenomic features that discriminate these carcinomas which exhibit different clinical behaviors.

Introduction:

One in eight women will be affected by an invasive breast cancer at some point in their lives. An estimated 232,340 new cases of breast cancer will affect women in 2013 and 39,620 women will die from the disease [ACS 2013]. Breast cancer presents itself in a variety of histologic types, and the two most common types are invasive ductal carcinoma (IDC) and invasive lobular carcinoma (ILC) [Corben 2013].

When a tumor is estrogen receptor positive (ER+), the growth can be controlled by one of two methods following the surgical excision of the tumor. The first is by blocking the estrogen receptor with an antiestrogen, such as the drug tamoxifen. The second method is to reduce the amount of estrogen in the body by inhibiting the conversion of estrogen's precursor to estrogen by the enzyme aromatase with aromatase inhibitor (AI) drugs, an example of which is letrozole [National Cancer Institute, 2010]. Although AIs are most effective in post-menopausal women, it has been found that different invasive breast carcinoma types have varied responses to letrozole [Metzger et al. 2012].

In a clinical setting, it is imperative to be able to properly distinguish between IDC and ILC, and we propose that a genomic marker can be utilized to aid in the distinction between the two histological subtypes when conventional pathologic tests are conflicting.

Figure 1 – Conflicting pathologic classification of an invasive breast carcinoma

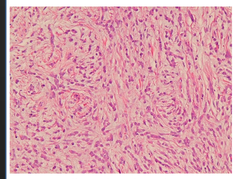

Hematoxylin and eosin stain illustrating ILC characteristics

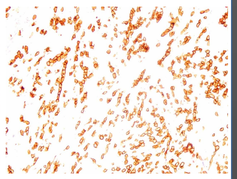

IHC stain for E-cadherin demonstrating IDC staining tendency

Figure 2 – Survival of varying grades IDC vs ILC

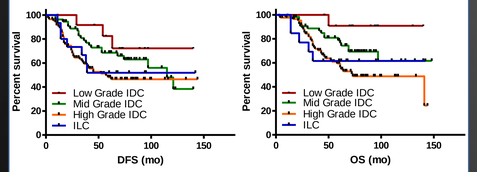

Materials and Methods:

Gene Selection

Genes were selected using microarray analyses of LCM-procured carcinoma cells from 247 de-identified human breast carcinoma biopsies. Of the 247 samples, 16 were ILC, 13 were low grade IDC, 55 were intermediate grade IDC and 85 were high grade IDC.

Initial analyses identified 1267 probes that were differentially expressed ($p<0.01$) between cell samples from patients with IDC compared to those with ILC. Gene expression levels in breast cancer cells from patients with low grade IDC compared to those with ILC yielded 200 sequences that were differentially expressed ($p<0.01$). When comparing high grade IDC to ILC, 149 of these genes were not differentially expressed.

Similar analysis were performed using only the microarray results from patients with ER+/PR+ cancers (n=107). Gene expression levels in carcinoma cells from patients with low grade IDC compared to ILC yielded 299 probe sequences ($p<0.01$). 99 of these genes were not differentially expressed when comparing high grade IDC to ILC ($p>0.01$). 15 genes were the same in the analysis of low grade IDC compared to ILC regardless of ER/PR status and in the same analysis with only ER/PR+ patient samples indicating that this gene set may serve as a panel of candidate genes. Of the 15 probes sequences, 12 genes were investigated further by qPCR.

Tissue Preparation & RNA Extraction

Using an IRB-approved study, frozen tissue sections from de-identified patients diagnosed with primary breast carcinoma and metastasis were utilized. Total RNA was extracted from frozen intact tissue sections with the RNeasy® Mini Kit (Qiagen Inc., Valencia, CA). Integrity of RNA was analyzed using the Bioanalyzer 2100 (Agilent Technologies, Palo Alto, CA). Total RNA was reverse transcribed using iScript (Biorad, Hercules, CA).

Gene Expression Analyses

Primers were designed using Primer Express (Applied Biosystems) and Primer Blast (NCBI). RNA quantification and analyses were performed in triplicate by qPCR in duplicate wells using the ABI Prism® 7900HT (Applied Biosystems, Foster City, CA) with Power Sybr® Green (Applied Biosystems) for detection. Relative gene expression was calculated using the ΔΔCt method with cDNA prepared from Universal Human Reference RNA (Stratagene, La Jolla, CA) as both a calibrator and a standard for quantification of RNA using β-actin (ACTB) as a reference gene.

Statistical Analysis

T-test, Kaplan Meier plots, Pearson correlations, and tumor marker analyses were performed in Graph Pad Prism. Cox regressions were performed in SPSS Statistics 21.

Figure 3 – Flow chart illustrating gene candidate selection process with microarray data

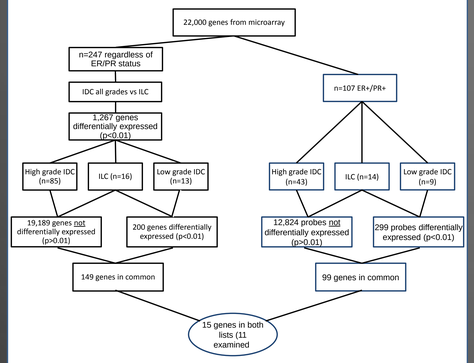

Table 1 – ER and PR protein levels exhibited in different histologic subtypes

ILC (n=97)		Grade 1 IDC (n=73)	
ER+/PR+	76 (78%)	ER+/PR+	54 (74%)
ER+/PR-	9 (10%)	ER+/PR-	14 (19%)
ER-/PR+	5 (5%)	ER-/PR+	4 (6%)
ER-/PR-	7 (7%)	ER-/PR-	1 (1%)

Grade 3 IDC (n=291)	
ER+/PR+	107 (37%)
ER+/PR-	21 (7%)
ER-/PR+	48 (16%)
ER-/PR-	115 (40%)

Fig 4 – ESR1 and PGR gene expression levels from microarray data in different histologic subtypes

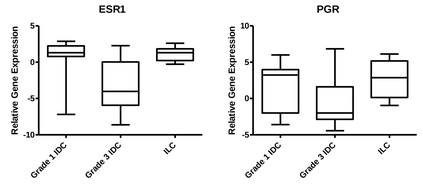

Fig 5 – Representative differences in gene expression levels of histologic subtypes using microarray data

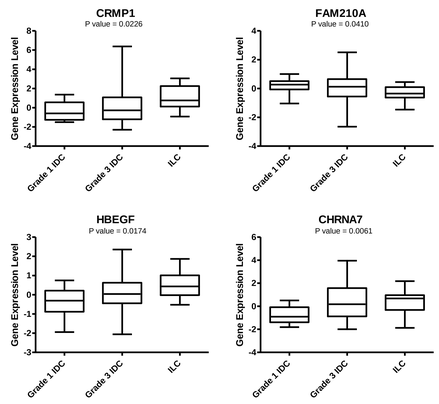

Table 2 – T-test of microarray data comparing gene candidate expression in Grade 1 IDC and ILC

Microarray Data

Gene	mean Grade 1 IDC	mean ILC	P value
BRWD1	0.425	-0.309	**0.005**
CAPSL	2.023	0.202	**0.010**
CHRNA7	-0.755	0.442	**0.002**
CMTM7	-1.443	0.212	**0.007**
CRMP1	-0.331	1.074	**0.009**
FAM210A	0.224	-0.328	**0.005**
GSKIP	0.378	-0.199	**0.011**
HBEGF	-0.376	0.512	**0.004**
HYMAI	-0.840	0.281	**0.008**
PAPPA - AJ420467	-0.200	0.431	**0.008**
PAPPA - AI271743	0.004	0.447	0.182
LRBA	0.533	-0.237	**0.004**

Table 3 – Pearson Correlation comparing expression results from microarray and qPCR of gene candidates

Pearson Correlation (n=29)

Gene	Pearson r	P value
BRWD1	0.1329	0.4918
CAPSL	0.5903	**0.0008**
CHRNA7	0.3615	0.054
CMTM7	0.7963	**< 0.0001**
CRMP1	0.2915	0.1249
FAM210A	0.05411	0.7804
GSKIP	0.1628	0.3987
HBEGF	0.6981	**< 0.0001**
HYMAI	0.4594	**0.0122**
PAPPA - AJ420467	0.08267	0.6698
PAPPA - AI271743	0.1512	0.4337
LRBA	-0.04324	0.8271

Fig 6 – Representative differences in gene expression levels of histologic types using qPCR data

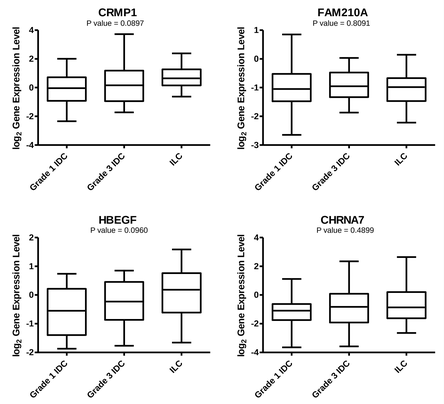

Table 4 – T-test of qPCR data comparing gene candidate expression in Grade 1 IDC and ILC

qPCR Data

Gene	mean Grade 1 IDC	mean ILC	P value
BRWD1	1.001	1.261	0.607
CAPSL	1.852	1.406	0.432
CHRNA7	-1.234	-0.670	0.255
CMTM7	-0.502	0.204	0.140
CRMP1	-0.078	0.733	**0.022**
FAM210A	-0.976	-1.030	0.787
GSKIP	0.669	1.009	0.233
HBEGF	-0.533	0.059	**0.036**
HYMAI	-2.082	-1.583	0.524
PAPPA	-1.579	-1.138	0.159
LRBA	1.689	2.096	0.375

Conclusions:

- **A gemonics-based test would assist pathologists when conventional pathologic tests to classify IDC and ILC are conflicting.**
- **ILC and Grade 1 IDC have varying overall and disease free survival with Grade 1 IDC receiving a more positive prognosis.**
- **Candidate genes were identified by analyzing the gene expression levels from microarray analyses using LCM-procured cancer cells.**
- **Grade 1 IDC and ILC exhibit similar ER and PR protein levels with the majority of the tumors being ER+/PR+.**
- **Grade 1 IDC and ILC have similar gene expression levels for the estrogen and progesterone receptors, reinforcing the need for a clinically relevant gene signature that would distinguish the two histologic subtypes.**
- **Gene expression levels are varied in the three histologic subtypes studied.**
- **T-tests using microarray gene expression level data were performed to find genes that are differentially expressed in Grade 1 IDC and ILC breast cancers.**
- **Gene expression levels retrieved from qPCR can be used to validate candidate genes that were identified by microarray assays.**
- **Two genes, CRMP1 and HBEGF, were identified as gene candidates and validated as significantly differentially expressed by qPCR.**
- **These two genes merit further investigation as potential clinically relevant biomarkers that would discriminate between invasive lobular and low grade invasive ductal breast carcinomas.**

Future Plans:

- **To examine the gene expression levels of candidate genes in tumors of patients who were treated specifically with letrozole following surgical excision of the tumors and compare these data with their clinical follow-up.**

References:

Metzger O, Giobbie-Hurder A, Mallon E, Viale G, Winer E, Thürlimann B, Gelber RD, Colleoni M, Ejlertsen B, Bonnefoi H, Coates AS, Goldhirsch A, Gusterson B. BIG 1-98 Collaborative Group, International Breast Cancer Study Group Relative effectiveness of letrozole compared with tamoxifen for patients with lobular carcinoma in the BIG 1-98 trial. Cancer Res 2012; 72(24 Suppl):Abstract nr S1-1

Reis-Filho JS , Simpson PT, Gale T., et al. The molecular genetics of breast cancer: the contribution of comparative genomic hybridization . Pathol Res Pract. 2005;201: 713-725.

American Cancer Society: CA, A Cancer Journal for Clinicians, 2013 Cancer Statistics

Corben, Adriana D., Pathology of Invasive Breast Disease, Surgical Clinics of North America, Volume 93, Issue 2, April 2013, Pages 363-392, ISSN 0039-6109, http://dx.doi.org/10.1016/j.suc.2013.01.003.

National Cancer Institute. (2010) Understanding Estrogen Receptors, Tamoxifen, and Raloxifene. Retrieved from http://www.cancer.gov/cancertopics/understandingcancer/estrogenreceptors/AllPages

Acknowledgements:

Supported in part by a grant from NIH/NCI R25-CA134283 and Phi Beta Psi Charity Trust.

Role of Exosomes in Tumor Growth and Metastasis

Cameron Campbell[a,b], Ramesh Gupta[a], Radha Munagala[a]

[a]Department of Pharmacology and Toxicology, University of Louisville and [b]Campbellsville University

BACKGROUND

- There will be an estimated 228,190 new cases, and 159,480 deaths, from lung cancer in the United States in 2013.[1]
- Cancer burdens and death are largely due to metastasis in several cancer types, including lung. Much effort has been put in to study how cancer cells metastasize.
- Emerging evidence implicates cancer cells undergo epithelial-mesenchymal transition (EMT) leading to enhanced cell migration and invasion abilities.
- Exosomes are endosome-derived 30-100 nm biological nanoparticles released from all types of cells but in abundance from tumor cells.
- Exosomes are released into the extracellular environment and have diverse biological functions. Contents of exosomes consist of proteins and genetic material (mRNA, DNA and miRNA) from the cell of origin. Exosomes can be taken up by other cells and induce both genetic and epigenetic changes.
- Tumor-derived exosomes have been reported to facilitate tumor growth, metastasis and drug resistance.[2]
- Understanding the role of tumor derived exosomes in cellular process would probably enable better management of cancer metastasis.

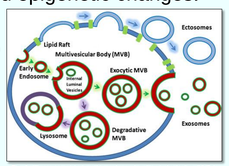

Fig. 1: "Exosomes originate within endosomal multivesicular bodies (MVBs), which are redirected to the cellular surface from the lysosomal degradation pathway." Taken from Lee, *et al.* 2011.

HYPOTHESIS

We hypothesize that <u>treatment of non-metastatic lung cancer cells with exosomes from metastatic cancers would increase growth rate, migratory behavior, and invasiveness of the non-aggressive cancer cells</u>. This would prove that exosomes carry the cargo essential for EMT transition leading to cancer metastasis.

RESULTS

Exosome Size Determination

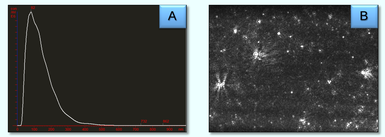

Fig. 2. A: Representative image for mode distribution of exosome size from H522. **B:** A representative field image of exosomes. Analyses were performed by NanoSight LM10 instrument.

Table 1: Mean and Mode Exosome Sizes

Cell Line	Mean size (nm)	Mode size (nm)
H522	140	82
A549	94	51
H1299	135	94

Uptake of A549- and H1299-released Exosomes by Non-invasive Lung Cancer H522 Cells

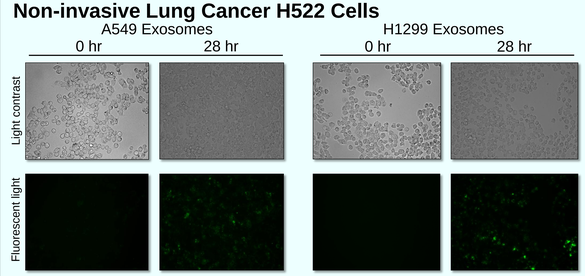

Fig. 3: Green fluorescent signals reflect incorporation of PKH-67 tagged exosomes into H522 cells. Over the course of 28 hr, the fluorescent signals of exosomes intensified with time. Signals were first detected at 20 hr in the H1299 treatment (not shown).

Wound Healing Assay

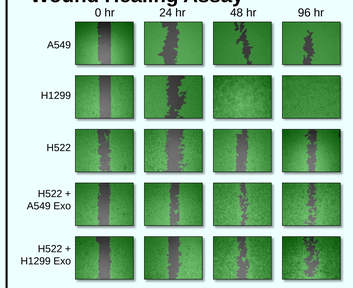

Fig. 4: Regions of cell growth are depicted in green. Gray areas represent absence of cells. Images were analyzed by Wimasis software.

Migration Assay

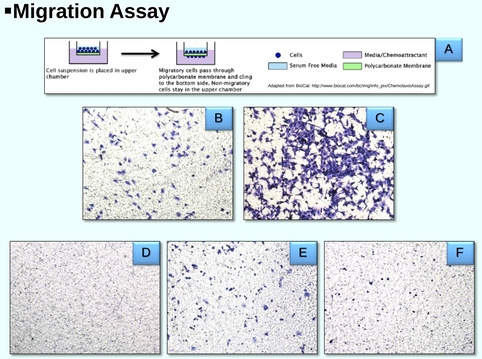

Fig. 5: Images were taken 48 hr after treatment. Cells were visualized after staining with 0.2% toluidine blue. **A:** Method of performing the migration assay. **B:** Migration of A549. **C:** Migration of H1299. **D:** Migration of H522 alone. **E:** Migration of H522 treated with A549 exosomes. **F:** Migration of H522 treated with H1299 exosomes.

Invasion Assay

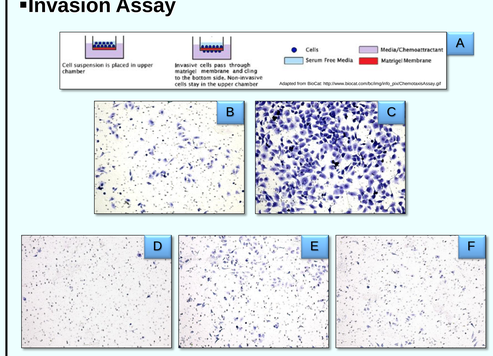

Fig. 6: Images were taken 48 hr after treatment. Cells were visualized after staining with 0.2% toluidine blue. **A:** Method of performing the invasion assay. **B:** Invasion of A549. **C:** Invasion of H1299. **D:** Invasion of H522 alone. **E:** Invasion of H522 treated with A549 exosomes. **F:** Invasion of H522 treated with H1299 exosomes.

Western Blot Analysis

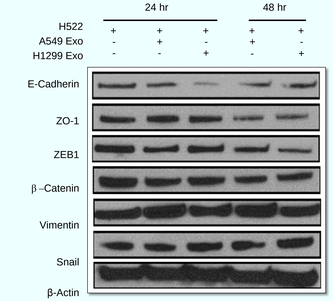

Fig. 7: Western blot analysis demonstrated the expression levels of proteins associated with epithelial-mesenchymal-transition shift. β-actin served as a control to show uniform protein loading.

KEY FINDINGS

- Exosomes isolated from the 3 lung cancer cell lines (H1299, A549 and H522) had a mean size of 94 – 162 nm (Fig. 2).
- The invasive and metastatic potential of the 3 lung cancer cell lines as observed by wound healing, migration and invasion assays in the descending order was as follows:

  H1299 > A549 >> H522
- Non-invasive H522 lung cancer cells could uptake the PKH-67 labeled exosomes from highly invasive A549 and H1299 cells as reflected by an increased fluorescent signal (Fig. 3).
- H522 treated with A549 or H1299 exosomes exhibited faster wound healing rate (Fig. 4), increased migratory behavior (Fig. 5), and invasiveness (Fig. 6). This indicates that exosomes carry the cargo essential for epithelial-mesenchymal-transition (EMT).
- H522 treated with A549 exosomes showed a greater metastatic shift than H1299 treatment.
- Analysis of key EMT-associated proteins in H522 cells treated with exosomes from A549 and H1299 cells indicated changes in expression levels favoring EMT. Expression levels of epithelial markers E-Cadherin, ZO-1, ZEB1, and β-Catenin were downregulated, whereas mesenchymal markers Vimentin and Snail were upregulated (Fig. 7).

SUMMARY

- Exosomes isolated from A549 and H1299 increased the metastatic potential of non-invasive H522 cells.
- Our findings provide insights of a possible role of exosomes in EMT of lung cancer cells.
- These findings make exosomes a promising platform for future research of EMT.
- Characterization of exosome components (protein, mRNA and miRNA) linked with EMT will be done in future studies.

METHODS

- **Exosome Isolation:** Conditioned media from H522, A549, and H1299 was collected after 72 hr in culture. Media was centrifuged sequentially to harvest exosomes (5,000g for 20 min; 120,000g for 17 hr). After washing with phosphate buffered saline (PBS), exosomes were dissolved in minimal volume (< 250 µL PBS).
- **Exosome Size Determination:** 100 µL samples of H522, A549, and H1299 exosome suspensions were injected into a NanoSight particle size microscope. Brownian movement was monitored via laser and used to determine particle sizes.
- **H522 Uptake of Exosomes:** PKH-67 fluorescent dye was diluted with diluent C (Sigma Aldrich, St. Louis, MO) and mixed with exosomes harvested from A549 and H1299 culture media. A total of 100 µg tagged A549 or H1299 exosomes were added to H522 cells. Uptake of exosomes by H522 cells was detected by green fluorescence over the course of 28 hr using a AMG EVOS fluorescent microscope (Invitrogen, Carlsbad, CA). Images were captured at 10x magnification.
- **Wound Healing Assay:** H1299, A549 and H522 cells with or without exosomes treatment were plated at a density of 7 x 10^5 cells/mL in a 30 µ-Dish with culture insert (Ibidi, Verona, WI). A total of 70 µL of cell suspension was added to both sides of the assay insert, which was removed after overnight incubation for cell attachment. H522 cells were further treated with 100 µg of either A549 exosomes or with H1299 exosomes. Wound healing was monitored over a period of 96 hr. Images were captured at 0, 24, 48 and 96 hr at 4x magnification using AMG EVOS microscope (Invitrogen, Carlsbad, CA). Images were analyzed using Wimasis software (Ibidi, Verona, WI). H1299 and A549 cells alone were plated to determine and compare wound healing capabilities between the cell lines.
- **Migration Assay:** Serum-free cell suspensions of 5 x 10^4 cells/mL density of A549, H1299, H522 alone, H522 with A549 exosomes, and H522 with H1299 exosomes were prepared. BD 24-well transwells received 500 µL of the cell suspensions and were placed in 1 mL of serum supplemented media. Wells for exosome treated samples received conditioned media from their respective cell lines. After 48 hr, transwells were rinsed in PBS, fixed in methanol, stained with 0.2% toluidine blue and air dried. Non-migrated cells were scraped from the upper surface of the membrane with a cotton swab, and migrated cells remaining on the bottom surface were viewed under inverted microscope (Nikon, Melville, NY) and images were captured at 10x magnification.
- **Invasion Assay:** Serum-free cell suspensions of 5 x 10^4 cells/mL density of A549, H1299, H522 alone, H522 with A549 exosomes, and H522 with H1299 exosomes were prepared. BD 24-well transwells received 300 µL of the cell suspensions and were placed in 1 mL of serum supplemented media. Wells for exosome treated samples received conditioned media from the respective exosome cell lines. After 48 hr, transwells were rinsed in PBS, fixed in 4% paraformaldehyde, stained with 0.2% toluidine blue and air dried. Non-migrated cells were scraped from the upper surface of the membrane with a cotton swab, and migrated cells remaining on the bottom surface were viewed under inverted microscope (Nikon, Melville, NY) and images were captured at 10x magnification.
- **Western Blot Analysis:** H522 cells were treated with 100 µg of A549 exosomes, or H1299 exosomes, for 24 hr and 48 hr. At the end of treatment cell lysates were prepared using RIPA lysis buffer supplemented with phosphatase and protease inhibitors as per manufacturers' instructions (Thermo Scientific, Waltham, MA). 50 µg protein was separated on SDS-PAGE gel, followed by transfer onto PVDF membrane. Membranes were blocked with 4% non-fat dry milk and probed with primary antibodies for select proteins (E-Cadherin, ZO-1, ZEB1, β-Catenin, Vimentin, and Snail) involved in epithelial-mesenchymal-transition (EMT) overnight at 4° C. After washing, membranes were incubated with HRP conjugated secondary antibody. Proteins were visualized with enhanced chemiluminescence detection kits (Thermo scientific, Waltham, MA).

REFERENCES

1. American Cancer Society. Cancer Facts & Figures 2013. Atlanta: American Cancer Society; 2013.
2. Muralidharan-Chari, V. *et al.* Microvesicles: mediators of extracellular communication during cancer progression. *Journal of Cell Science*, **2010**, *123*, 1603-1611.
3. Lee, T. *et al.* Microvesicles as mediators of intercellular communication in cancer—the emerging science of cellular debris. *Springer-Verlag*, **2011**, *33*, 455-467.

ACKNOWLEDGEMENTS

Supported by grant R25- CA-134283 from the National Cancer Institute.

Role of Tumor Cell – Stromal Interactions on TGFβ-1 Mediated Gene Expression

M Cook[1], JD Ritzenthaler[2], J Roman[1,2,3]

[1]Department of Pharmacology and Toxicology; [2]Department of Medicine; and [3]Louisville VA Medical Center, Louisville KY

ABSTRACT

The extracellular matrix (ECM) plays an important role in the growth, proliferation, and metastasis of tumor cells. These effects have been linked to the activity of the cytokine transforming growth factor beta (TGFβ-1). Among other things, TGFβ-1 has also been shown to be involved with the development and progression of lung cancer, the leading cause of cancer-related deaths in the United States. What is not completely understood is how TGFβ-1 and the ECM interact to promote the development of cancer. We hypothesize that tumor cell–stromal interactions modulate TGFβ-1 induced gene expression, and tested these interactions in murine primary lung fibroblasts and in Lewis Lung Carcinoma (LLC). First, we showed that TGFβ-1 stimulated the proliferation of cells and that this was affected by the ECM. Second, we showed that LLC cells expressed SMAD3 and α-SMA mRNA in response to TGFβ-1 and that this was enhanced when cells were grown on the ECM molecule fibronectin (FN). Third, Western blot analysis showed that SMAD3 protein levels were further elevated in TGFβ-1 treated LLC and fibroblast cells grown on collagen type I (Coll I) and FN. Importantly, we found that SMAD3 nuclear binding to the α-SMA gene promoter increased in TGFβ-1 treated cells, and this was modulated by ECM. We conclude that ECMs indeed influence TGFβ-1 /SMAD3 – dependent gene expression.

HYPOTHESIS

Tumor cell–stromal interactions modulate TGFβ-1 induced gene expression.

METHODS

RT-PCR. Cells were plated onto 6 well plates (4 x 10^4 cells/well), incubated for 24 h followed by washing and then harvested and processed for mRNA isolation. RT reactions were performed using specific primers. The PCR protocol was: 95°C for 30 sec, 60°C for 30 sec, 72°C for 1 min. for 45 cycles. PCR products were resolved on 1% agarose gels. **Western Blot.** Cells were washed, lysed in homogenization buffer and cell extract (20 µg of protein) was mixed with 2x sample buffer, and resolved on a 10% SDS polyacrylamide gel for 1 h at 150 V. Proteins were transferred onto nitrocellulose for 2 h at 25 mA, blocked with blotto for 1 h, and washed. Blots were incubated with primary antibody for 24 h at 4°C, washed, incubated with secondary goat anti-rabbit IgG (HRP-conjugated) for 1.5 h at room temperature. Blots were washed, transferred to ECL solution for 1 min., and exposed to X-ray film. Protein bands were quantified by densitometry using a Bio-Rad GS-800 laser densitometer (Hercules, CA). **Cell viability assay.** Primary lung fibroblasts and LLCs (1 x 10^4 cells/ml) were added to 96-well tissue culture plates and incubated with for 24-120 h. Luminescence of viable cells was detected using Cell Titer-Glo Luminescent Cell Viability Assay Kit according to the manufacturer (Promega, Madison, WI). Quantification was performed using a Labsystems Luminoskan Ascent Plate Luminometer. ChIP Assay. 10 x10^6 cells were grown on 150 mm_2 plates coated with Poly-L-Lysine, collagen I, or fibronectin and treated with 5 ng/µl TGFβ-1 for 6 h. Cells were washed, harvested, and processed for immunoprecipitation and PCR.

RESULTS

I. DNA binding by SMADs in fibroblasts is differentially affected by Coll I and FN as determined by EMSA (A). This is important considering that tumor cells are immersed in FN (B vs. C) and other matrices.

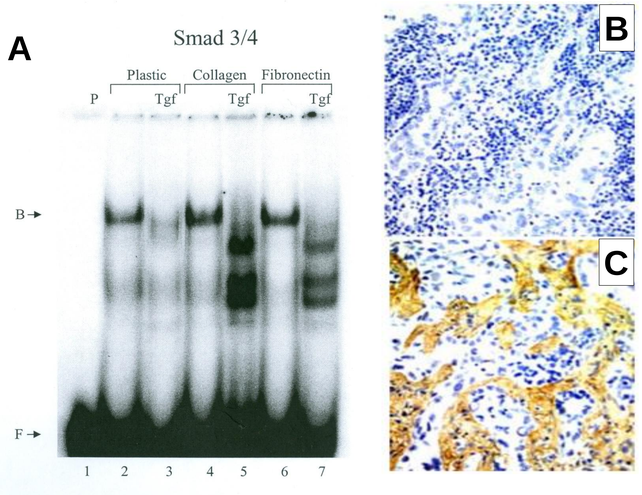

II. Matrix affects TGFβ-1 mediated α-SMA and SMAD3 mRNA expression per RT-PCR

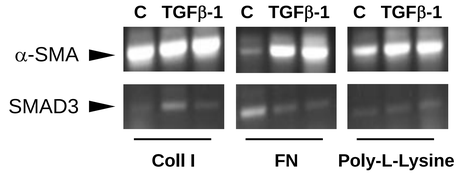

III.TGFβ-1 induces increased SMAD3 protein expression per Western Blotting

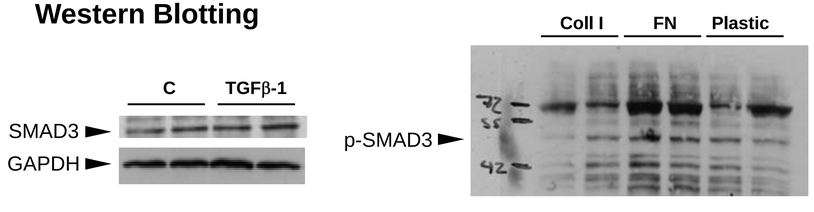

IV. Collagen I and fibronectin ECMs stimulate fibroblast (A) and cancer cell (B) proliferation

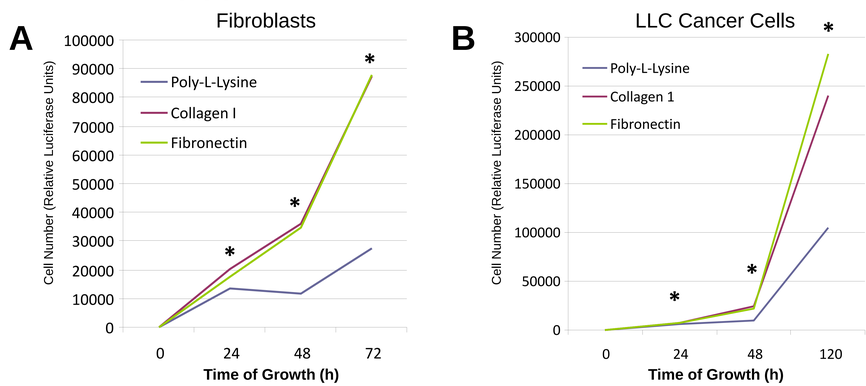

V. SMAD3 DNA binding increased in two different regions of the α-SMA promoter in response to TGFβ-1 and this is modulated by ECM

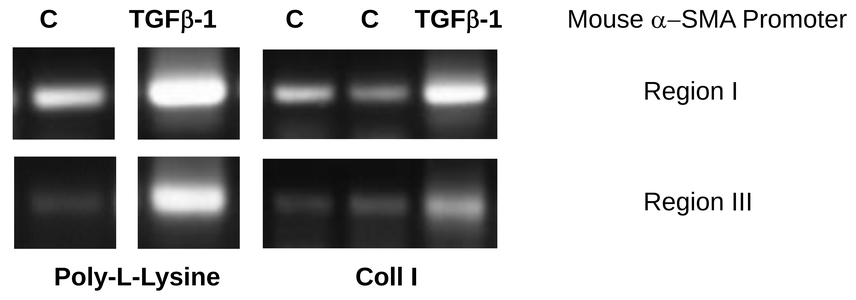

CONCLUSIONS & ACKNOWLEDGMENTS

We conclude that ECM composition may influence SMAD3 expression and SMAD3 DNA binding in response to TGFβ-1 which, in turn, affects cellular processes such as proliferation.

This is important considering that lung cancer often originates in patients with abnormal lungs that show increased deposition of ECMs FN and Coll I.

Further work will be directed at identifying how ECMs may affect the TGFβ-1/SMAD3 pathway by modulating TGFβ-1 receptor signaling and the identify of other nuclear binding proteins which, ultimately, affect SMAD3 binding and gene regulation in the conditions described above.

This work was supported by NIH/NCI grant R25-CA134283